Inorg. Chem. **2005**, *44*, 3684–3689

$La_9Sb_{16}Br_3$ and $Ce_9Sb_{16}Cl_3$: Stars and Stripes in Rare Earth Halide and Intermetallic Compounds†

Chong Zheng,*,‡ Hansjürgen Mattausch,§ and Arndt Simon§

Department of Chemistry and Biochemistry, Northern Illinois University, DeKalb, Illinois 60115, and Max-Planck-Institut für Festkörperforschung, Heisenbergstrasse 1, D-70569 Stuttgart, Germany

Received June 15, 2004

The title compounds were synthesized from Ln, LnX_3 (Ln = La, Ce; X = Cl, Br), and Sb under an Ar atmosphere at 950 °C. They crystallize in the space group $P6_3/m$ (No. 176) with lattice constants a = 21.232(5) and 20.862(2) Å and c = 4.323(2) and 4.2728(7) Å for $La_9Sb_{16}Br_3$ and $Ce_9Sb_{16}Cl_3$, respectively. The solids are the most metal-rich members in the reduced rare earth metal halide family and contain partial structures which are characteristic of reduced halides and intermetallic phases. These are the $[Ln_6X_6]_\infty$ hexagon stars, Sb-centered $[Ln_3Sb]_\infty$ trigonal prismatic columns, and stripes of Sb square meshes. Computational analysis indicates that their electronic structure is valence-precise in the reduced halide part, but electron-deficient in the intermetallic part. Susceptibility and resistivity measurements reveal the metallic nature of the compounds.

Introduction

Rare earth metal halides and intermetallic compounds are important to the development, fabrication, and application of electronic materials.[1−5] Reduced rare earth halides are particularly interesting for their chemical and structural diversity. A prominent feature of the reduced rare earth halides is their hosting capability. A plethora of interstitials with vastly different electronic properties can be accommodated at the center of a rare earth metal octahedron or trigonal prism, just to mention the most frequent polyhedra. These guests range from the main group elements H, B, Al, Ga, C, Si, Ge, N, P, As, and Sb to the transition metals Mn, Fe, Co, Ni, Ru, Os, Rh, Ir, and Pt.[6−17] The electronic requirement for these reduced halides, however, is rather stringent. Only a narrow band in the rare earth d block, arising from interaction with interstitial orbitals, contributes to metal−metal bonding, and a restriction of no more than one skeleton electron per rare earth atom is bestowed upon.[18] In the case of rare earth halides without interstitials, the requirement can be relaxed, as in the case of Gd_2Cl_3 and LaI.[19,20] In contrast, intermetallic compounds can have many delocalized bonding states, allowing a large range of filling by electrons as exemplified by the Nowotny phases.[21−29] Part

* To whom correspondence should be addressed. E-mail: zheng@cz.chem.niu.edu.

† Dedicated to Prof. Roald Hoffmann in admiration of his insight to chemical bonding.

‡ Northern Illinois University.

§ Max-Planck-Institut für Festkörperforschung.

(1) Rao, C. N. R.; Cheetham, A. K. *Science* **1996**, *272*, 369.
(2) Chuang, Y.-D.; Gromko, A. D.; Dessau, D. S.; Kimura, T.; Tokura, Y. *Science* **2001**, *292*, 1509.
(3) Orenstein, J.; Millis, A. J. *Science* **2000**, *288*, 468.
(4) Kasuya, T.; Saso, T. *Theory of Heavy Fermions and Valence Fluctuations*; Springer-Verlag: New York, 1985.
(5) Stewart, G. R. *Rev. Mod. Phys.* **1984**, *56*, 755.
(6) Simon, A.; Mattausch, Hj.; Miller, G. J.; Bauhofer, W.; Kremer, R. K. *Handbook on the Physics and Chemistry of Rare Earths;* Elsevier Science Publishers: Amsterdam, 1991; Vol. 15, pp 191−285.
(7) Mattausch, Hj.; Oeckler, O.; Simon, A. *Inorg. Chim. Acta* **1999**, *289*, 174.
(8) Mattausch, Hj.; Simon, A. *Angew. Chem.* **1998**, *110*, 498; *Angew. Chem., Int. Ed.* **1998**, *37*, 499.
(9) Warkentin, E.; Simon, A. *Rev. Chim. Miner.* **1983**, *20*, 488.
(10) Nagaki, D.; Simon, A.; Borrmann, H. *J. Less-Common Met.* **1989**, *156*, 193.
(11) Dorhout, P. K.; Payne, M. W.; Corbett, J. D. *Inorg. Chem.* **1991**, *30*, 4960.
(12) Llusar, R.; Corbett, J. D. *Inorg. Chem.* **1994**, *33*, 849.
(13) Hughbanks, T.; Rosenthal, G.; Corbett, J. D. *J. Am. Chem. Soc.* **1986**, *108*, 8289.
(14) Hughbanks, T.; Corbett, J. D. *Inorg. Chem.* **1988**, *27*, 2022.
(15) Hughbanks, T.; Corbett, J. D. *Inorg. Chem.* **1989**, *28*, 631.
(16) Meyer, G.; Wickleder, M. S. *Handbook on the Physics and Chemistry of Rare Earths*; Elsevier Science Publishers: Amsterdam, 2000; Vol. 28, Chapter 177, pp 53−129.
(17) Corbett, J. D. *J. Chem. Soc., Dalton Trans.* **1996**, 575.
(18) Zheng, C.; Oeckler, O.; Mattausch, Hj.; Simon, A. *Z. Anorg. Allg. Chem.* **2001**, *627*, 2151.
(19) Martin, J. D.; Corbett, J. D. *Angew. Chem.* **1995**, *107*, 234.
(20) Simon, A.; Holzer, N.; Mattausch, Hj. *Z. Anorg. Allg. Chem.* **1979**, *456*, 207.
(21) Jeitschko, W.; Parthé, E. *Acta Crystallogr.* **1967**, *22*, 551.
(22) Nowotny, H.; Lux, B.; Kudielka, H. *Monatsh. Chem.* **1956**, *87*, 447.

10.1021/ic049220u CCC: $30.25
Published on Web 04/13/2005

of our recent research has been focusing on the metal-rich side of the reduced rare earth halides. Compounds consisting of both reduced halide and intermetallic components are of particular interest, as the halide hosting capability can allow fine-tuning of the electronic structures to produce desired physical effects such as superconductivity and magnetoresistance.[30−32] By combining with intermetallic components, these hybrid compounds provide still further flexibility in their electronic structure and in turn potentially more physical effect possibilities. In this contribution, we report two such metal-rich compounds $Ln_9Sb_{16}X_3$ (Ln = La, Ce; X = Cl, Br). With a metal/metalloid-to-nonmetal ratio of 8.3, they are the most metal-rich members in the reduced rare earth metal halide family. The chemical synthesis, structure determination, computational analysis of their electronic structure, and physical property measurements are reported.

Experimental Section

Synthesis. Ln metals (Ln = La, Ce) (sublimed, 99.99%; Alfa-Aesar, small pieces), LnX_3 (X = Cl, Br), and Sb (99.99%; Aldrich) were used as starting materials. $LaBr_3$ was synthesized from the reaction of La_2O_3 with NH_4Br and HBr (48% concentration). $CeCl_3$ was obtained from the reaction of Ce metal with HCl (37%). The products $LaBr_3$ and $CeCl_3$ were purified twice by sublimation in a Ta tube before being used. All handling was carried out under an Ar atmosphere either in a glovebox or through the Schlenk technique.

The stoichiometric mixtures (ca. 1.5 g) of the starting materials were arc-sealed in Ta tubes under an Ar atmosphere. The Ta tubes were then sealed inside silica glass ampules under a vacuum of ca. 10^{-2} mbar. The reaction temperatures and times were 950 °C and 7 days for $La_9Sb_{16}Br_3$ and 950 °C and 18 days for $Ce_9Sb_{16}Cl_3$. After the reactions, the ampules were opened under an Ar atmosphere. Many metallic golden thin needle-shaped single crystals were observed in the products. These crystals are not air- or moisture-sensitive, but subsequent handling was carried out under an Ar atmosphere as a precaution. The yield, estimated from Guinier measurements, was greater than 90%. EDX analyses of these single crystals, using a JEOL JSM-6510LV scanning electron microscope, confirmed the presence of the component elements in the average atomic ratio of 31:48:12 (Ln:Sb:X) with an uncertainty of approximately 5% associated with this method.

Structural Determination. The reaction products were ground to fine powders under an Ar atmosphere and sealed in glass capillaries for phase identification by a modified Guinier technique[33] (Cu $K\alpha_1$: $\lambda = 1.54056$ Å; internal standard Si with $a = 5.43035$ Å; Fujifilm BAS-5000 image plate system). Single crystals were transferred to glass capillaries under Na-dried paraffin oil and sealed under an Ar atmosphere. They were first examined by precession and Weissenberg techniques before being characterized on a Bruker CCD diffractometer. The structure was solved with direct methods using the SHELXS and SIR97 programs.[34−36] Full-matrix least-squares refinement on F^2 was carried out using the SHELXTL program.[35]

Table 1. Crystal Data and Structure Refinement for $La_9Sb_{16}Br_3$ and $Ce_9Sb_{16}Cl_3$ (Unit Cell Dimensions Are Derived from Single-Crystal Data)

empirical formula	$La_9Sb_{16}Br_3$	$Ce_9Sb_{16}Cl_3$
fw	3437.92	3315.43
temp (K)	293(2)	293(2)
wavelength (Å)	0.71073	0.71073
cryst syst	hexagonal	hexagonal
space group	$P6_3/m$ (No. 176)	$P6_3/m$ (No. 176)
unit cell dimensions (Å)		
a:	21.232(5)	20.862(2)
c:	4.323(2)	4.2728(7)
vol (Å^3), Z	1687.5(10), 2	1610.5(3), 2
density (g/cm^3, calculated)	6.766	6.837
absorption coeff (mm^{-1})	27.202	25.812
independent data/parameters	1130/58	979/58
GOF on F^2	1.608	1.486
final *R* indices[a] [$I > 2\sigma I$)]		
R1:	0.0411	0.0519
wR2:	0.0866	0.1043

[a] $R1 = \sum||F_o| - |F_c||/\sum|F_o|$; $wR2 = [\sum[w(F_o^2 - F_c^2)^2]/\sum[w(F_o^2)^2]]^{1/2}$.

The product compounds crystallize in the hexagonal lattice with space group $P6_3/m$ (No. 176) and $Z = 2$. The crystallographic information including the fractional coordinates and selected bond lengths of these compounds is listed in Tables 1−3.

Computational Study. The density of states (DOS) and the crystal orbital overlap population (COOP)[37] curves were computed using both the tight-binding extended Hückel method (EH)[38,39] and the self-consistent linear muffin-tin orbital density functional scheme using the local density approximation (LDA) as implemented in the Stuttgart-TB-LMTO-ASA program.[40] The electron localization function (ELF)[41−47] was also calculated using the LDA method. Approximately 200 k-points in the irreducible wedge of the Brillouin zone were used in the EH computation of the DOS and COOP curves. More than 1000 k-points in the whole Brillouin zone were generated in the LDA calculations. These k-points were then

(23) Jeitschko, W.; Nowotny, H.; Benesovsky, F. *Monatsh. Chem.* **1963**, *94*, 844.
(24) Jeitschko, W.; Nowotny, H.; Benesovsky, F. *Monatsh. Chem.* **1964**, *95*, 1242.
(25) Nowotny, H.; Benesovsky, F. *Phase Stability in Metals and Alloys*; McGraw-Hill: New York, 1967; p 319.
(26) Corbett, J. D.; Garcia, E.; Guloy, A. M.; Hurng, W.-M.; Kwon, Y.-U.; Leon-Escamilla, E. A. *Chem. Mater.* **1998**, *10*, 2824.
(27) Kwon, Y.-U.; Rzeznik, M. A.; Guloy, A.; Corbett, J. D. *Chem. Mater.* **1990**, *2*, 546.
(28) Maggard, P. A.; Corbett, J. D. *Inorg. Chem.* **2001**, *40*, 1352.
(29) Zheng, C.; Mattausch, Hj.; Simon, A. *J. Alloys Compds.* **2002**, *347*, 79.
(30) Simon, A.; Mattausch, Hj.; Eger, R.; Kremer, R. K. *Angew. Chem.* **1991**, *103*, 1209; *Angew. Chem., Int. Ed. Engl.* **1991**, *30*, 1188.
(31) Felser, C.; Ahn, K.; Kremer, R. K.; Seshadri, R.; Simon, A. *J. Solid State Chem.* **1999**, *147*, 19.
(32) Kremer, R. K.; Cockcroft, J. K.; Mattausch, Hj.; Schnelle, W.; Simon, A. *J. Magn. Magn. Mater.* **1995**, *140−144*, 1187.
(33) Simon, A. *J. Appl. Crystallogr.* **1970**, *3*, 11.
(34) Sheldrick, G. M. *SHELXS-97, Program for the Solution of Crystal Structures*; Universität Göttingen: Göttingen, Germany, 1997.
(35) Sheldrick, G. M. *SHELXTL. Version 5.1*; Siemens Analytical Instruments Inc.: Madison, WI, 1997.
(36) Altomare, A.; Burla, M. C.; Camalli, M.; Cascarano, G. L.; Giacovazzo, C.; Guagliardi, A.; Moliterni, A. G. G.; Polidori, G.; Spagna, R. *J. Appl. Crystallogr.* **1999**, *32*, 115.
(37) Wijeyesekera, S. D.; Hoffmann, R. *Organometallics* **1984**, *3*, 949.
(38) Whangbo, M. H.; Hoffmann, R.; Woodward, R. B. *Proc. R. Soc. London* **1979**, *A366*, 23.
(39) Hoffmann, R. *J. Chem. Phys.* **1963**, *39*, 1397.
(40) Andersen, O. K.; Jepsen, O. *Phys. Rev. Lett.* **1984**, *53*, 2571.
(41) Savin, A.; Becke, A. D.; Flad, J.; Nesper, R.; Preuss, H.; von Schnering, H. G. *Angew. Chem.* **1991**, *103*, 421.
(42) Savin, A.; Flad, H.-J.; Flad, J.; Preuss, H.; von Schnering, H. G. *Angew. Chem.* **1992**, *104*, 185.
(43) Faessler, T. F.; Savin, A. *Chem. Unserer Zeit* **1997**, *31*, 110.
(44) Alikhami, M. E.; Bouteiller, Y.; Silvi, B. *J. Phys. Chem.* **1996**, *100*, 16092.
(45) Becke, A. D.; Edgecomb, K. E. *J. Chem. Phys.* **1990**, *92*, 5397.
(46) Savin, A.; Nesper, R.; Wengert, S.; Faessler, T. F. *Angew. Chem.* **1997**, *109*, 1892; *Angew. Chem., Int. Ed. Engl.* **1997**, *36*, 1808.
(47) Silvi, B.; Savin, A. *Nature* **1994**, *371*, 683.

Table 2. Atomic Coordinates ($\times 10^4$) and Equivalent Isotropic Displacement Parameters ($Å^2 \times 10^3$) for $La_9Sb_{16}Br_3$ and $Ce_9Sb_{16}Cl_3$

	Wyckoff position	x	y	z	U(eq)[a]
		$La_9Sb_{16}Br_3$			
La(1)	6h	5418(1)	3091(1)	2500	12(1)
La(2)	6h	1518(1)	2464(1)	2500	14(1)
La(3)	6h	3940(1)	4013(1)	2500	13(1)
Sb(1)	2c	3333	6667	2500	13(1)
Sb(2)	6h	4846(1)	5879(1)	2500	14(1)
Sb(3)	6h	5085(1)	1368(1)	2500	16(1)
Sb(4)	6h	2501(1)	4287(1)	2500	13(1)
Sb(5)	6h	3574(1)	2258(1)	2500	16(1)
Sb(6)	6h	95(1)	2850(1)	2500	15(1)
Br	6h	1480(1)	981(1)	2500	18(1)
		$Ce_9Sb_{16}Cl_3$			
Ce(1)	6h	5406(1)	3087(1)	2500	9(1)
Ce(2)	6h	1441(1)	2380(1)	2500	10(1)
Ce(3)	6h	3923(1)	4002(1)	2500	11(1)
Sb(1)	2c	3333	6667	2500	10(1)
Sb(2)	6h	4867(1)	5894(1)	2500	11(1)
Sb(3)	6h	5083(1)	1368(1)	2500	13(1)
Sb(4)	6h	2478(1)	4255(1)	2500	11(1)
Sb(5)	6h	3534(1)	2245(1)	2500	12(1)
Sb(6)	6h	49(1)	2801(1)	2500	13(1)
Cl	6h	1475(4)	985(4)	2500	17(2)

[a] U(eq) is defined as one-third of the trace of the orthogonalized U_{ij} tensor.

Table 3. Selected Bond Lengths [Å] for $Ln_9Sb_{16}X_3$ (Ln = La, Ce; X = Cl, Br)[a]

	coordination	$La_9Sb_{16}Br_3$	$Ce_9Sb_{16}Cl_3$
Ln(1)−Sb(1)#1	Sb(1) in TP	3.256(1)	3.225(1)
Ln(1)−Sb(2)#1	Ln(1) to edge of ST	3.316(2)	3.257(2)
Ln(1)−Sb(3)#3	Ln(1) to ST	3.356(2)	3.307(2)
Ln(1)−Sb(3)	Ln(1) to ST	3.360(2)	3.303(2)
Ln(1)−Sb(4)#4	Ln(1) to center of ST	3.384(2)	3.352(2)
Ln(1)−Sb(5)	Ln(1) to ST	3.395(2)	3.386(2)
Ln(1)−Ln(1)#3	Ln(1) triangle in TP	4.218(2)	4.184(3)
Ln(2)−X#7	outer corner to inner corner of S	3.032(2)	2.884(5)
Ln(2)−X	outer corner to inner corner of S	3.111(3)	2.947(8)
Ln(2)−Sb(4)	S corner to ST center	3.355(2)	3.394(2)
Ln(2)−Sb(6)#4	S corner to ST edge	3.363(2)	3.319(2)
Ln(2)−Sb(5)#7	S corner to ST	3.379(2)	3.351(2)
Ln(2)−Sb(6)	S corner to ST edge	3.502(2)	3.430(3)
Ln(3)−Sb(2)#1	Ln(3) to ST edge	3.282(2)	3.231(2)
Ln(3)−Sb(6)#4	Ln(3) to ST edge	3.314(2)	3.276(2)
Ln(3)−Sb(3)#7	Ln(3) to ST	3.341(2)	3.289(2)
Ln(3)−Sb(4)	Ln(3) to ST center	3.386(2)	3.310(2)
Ln(3)−Sb(5)	Ln(3) to ST	3.404(2)	3.334(2)
Ln(3)−Sb(2)	Ln(3) to ST edge	3.432(2)	3.418(2)
Sb(2)−Sb(3)#7	Sb(3) at Sb(2), Sb(4) SP	3.037(2)	3.022(2)
Sb(3)−Sb(4)#4	Sb(3) at Sb(2), Sb(4) SP	3.136(2)	3.122(2)
Sb(4)−Sb(5)#7	Sb(4) at Sb(3), Sb(5) SP	3.079(2)	3.041(2)
Sb(4)−Sb(3)#7	Sb(4) at Sb(3), Sb(5) SP	3.136(2)	3.122(2)
Sb(5)−Sb(6)#4	Sb(5) at Sb(4), Sb(4) SP	3.125(2)	3.105(2)

symmetry transformations used to generate equivalent atoms:
#1 $-x+1, -y+1, -z+1$; #3 $-x+y+1, -x+1, z$;
#4 $y, -x+y, -z$; #7 $x-y, x, -z$

[a] Atomic coordinations are also indicated in the table (TP for $Ln(1)_6$ trigonal prism; ST for Sb stripe, S for Ln_6X_6 star, and SP for Sb_4 square planar).

reduced to the irreducible wedge of the Brillouin zone. The EH parameters used in the computation are listed in Table 4.

Physical Property Measurements. For conductivity measurement, the polycrystalline samples were pressed into pellets of 5 mm in diameter and ca. 2 mm in thickness. The conventional four-contact method[48] was used. Susceptibility measurements were carried out on a Quantum Design PPMS 6000 magnetometer, using sample quantities of ca. 50 mg.

(48) van der Pauw, L. J. *Philips Res. Rev.* **1958**, *13*, 1.

Table 4. Extended Hückel Parameters

	orbital	H_{ii} (eV)	ζ_1[a]	ζ_2	c_1[a]	c_2
La	6s	−7.67	2.14			
	6p	−5.01	2.08			
	5d	−8.21	3.78	1.381	0.7765	0.4586
Sb	5s	−18.8	2.323			
	5p	−11.7	1.999			
Br	4s	−22.07	2.588			
	4p	−13.1	2.131			

[a] Exponents and coefficients in a double ζ expansion of the d orbital.

Results and Discussion

Crystal Structure. $La_9Sb_{16}Br_3$ and $Ce_9Sb_{16}Cl_3$ are the most metal/metalloid-rich compound in the reduced rare earth halide family. With a metal/metalloid-to-nonmetal ratio (M:X) of 8.3, they compare with the Nowotny phase La_5Sn_3X (X = Cl, Br, I; M:X = 8),[21,26,29] most rare earth metal-rich ternary chalcogenide $Er_7Ni_2Te_2$ (M:X = 4.5),[49] and the metal-rich non rare earth compounds $Bi_{12}Rh_3Br_2$ (M:X = 7.5).[50] The compounds reported here represent a new structure type. Their structure consists of $[Ln_6X_6]_\infty$ (X = Br, Cl) hexagon stars, Sb-centered $[Ln_3Sb]_\infty$ (Ln = La, Ce) trigonal prismatic columns, and Ln-capped Sb square net stripes (Figure 1). The stars, trigonal prismatic columns, and the Sb stripes all run parallel to the *c*-axis. The stars and trigonal prisms are reminiscent of structural features that are usually associated with reduced rare earth halides. The stripe is infinitely long and four Sb row wide with an edge-to-edge distance of ca. 8.85 Å. Three of these stripes surround a trigonal prism. The closest contact between two stripes, measured from an edge Sb atom of one stripe to a center Sb atom of another, is ca. 4.269 Å. There are three crystallographically different Ln atoms in the structure (Table 2). Ln1 forms the trigonal prism, Ln2 the $[Ln_6X_6]_\infty$ star, and the Ln3 chain runs parallel to the *c*-axis. The Ln3 atom is located at the center of a distorted Sb_6 trigonal prism with the triangular edges ranging from 4.261 to 4.444 Å. The three rectangular faces of the prism are capped by still another three Sb atoms. Thus, the coordination of the Ln3 atom can be described as 6+3. There are six types of Sb atoms. Sb1 (Sb_i in Figure 1a) is at the center of the $[Ln_3Sb]_\infty$ trigonal prismatic column. Sb2 through Sb6 are in the stripes. Sb2 and Sb6 (Sb_e in Figure 1b) are at the edges of the Sb stripes. Sb3 and Sb5 are adjacent to the center, and Sb4 is in the middle of the stripes (Sb_c in Figure 1b). All atoms have a multiplicity of 6 except for Sb1 which has a multiplicity of 2, giving rise to the reported stoichiometry. In $La_9Sb_{16}Br_3$, the La−Sb_i distance in the $[La_3Sb]_\infty$ trigonal prism (La1−Sb1#1 in Table 3) is 3.256 Å. The La−Sb distances in the La-capped Sb square nets range from 3.314 to 3.502 Å. Although they are much larger than the sum of covalent radii of La and Sb (1.69 Å + 1.41 Å in Pauling scale) for a single bond, these contacts indicate delocalized covalent bonding considering their high coordination numbers. There are two La−Br bond lengths (La2−Br#7 and La2−Br in Table 3) in the $[La_6Br_6]_\infty$ star, 3.032 and 3.111 Å. These correspond to strong La−Br

(49) Meng, F.; Hughbanks, T. *Inorg. Chem.* **2001**, *40*, 2482.
(50) Ruck, M. *Solid State Sci.* **2001**, *3*, 369.

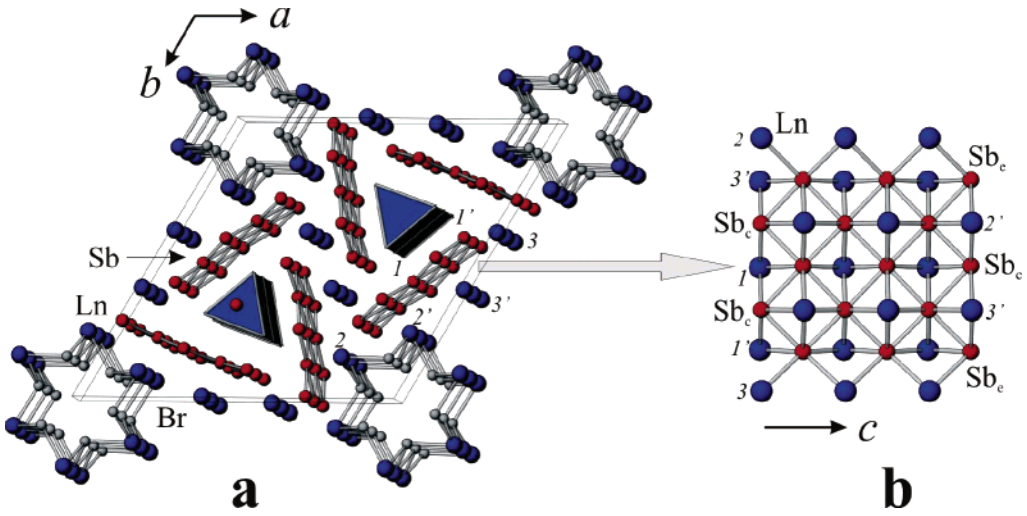

Figure 1. (a) The $Ln_9Sb_{16}X_3$ (Ln = La, Ce; X = Cl, Br) structure viewed down the *c*-axis. It consists of $[Ln_6X_6]_\infty$ hexagon stars centered at the cell corners (Ln in blue and X gray) and Sb-centered $[Ln_3Sb]_\infty$ trigonal prismatic columns (blue) each surrounded by three Ln-capped Sb square stripes (red) parallel to the *c*-axis. A third type of Ln (Ln3 in Tables 2 and 3) forms chains parallel to the *c*-axis with a spacing of the *c*-axis length (4.323 Å for $La_9Sb_{16}Br_3$). It is coordinated in a 6+3 fashion. The edge-to-center distances between two Sb stripes surrounding a $[Ln_3Sb]_\infty$ trigonal prism is ca. 4.269 Å for $La_9Sb_{16}Br_3$. (b) A Ln-capped Sb square net in the $Ln_9Sb_{16}Br_3$ structure. Sb_e is at the edge and Sb_c are in the middle of the Sb square meshed stripes. Corresponding Ln atoms in Figure 1a and Figure 1b are labeled by numbers.

bonding. The La−La distances in the trigonal prism range from 4.218 Å (within the La_3 triangle perpendicular to the column) to 4.323 Å (between La_3 triangles). These long distances imply weak La−La bonding. The Sb−Sb distances in the square net vary from 3.037 to 3.136 Å, longer than the sum of covalent radii of two Sb atoms. These contacts can also be considered as covalent bonds, and their length is due to the high coordination number. The structural feature is similar in $Ce_9Sb_{16}Cl_3$.

The coordination number (CN) for each Sb atom in the stripe is also of interest to the analysis of the electronic structure of the title compounds. For the edge Sb atoms (Sb2 and Sb6), CN = 5 (Sb2−La3 = 3.282 Å (2×), Sb2−La1 = 3.316 Å (2×), Sb2−La3 = 3.432 Å); Sb6−La3 = 3.314 Å (2×), Sb6−La2 = 3.363 Å (2×), Sb6−La2 = 3.502 Å for $La_9Sb_{16}Br_3$); for the near-center Sb atoms (Sb3 and Sb5), CN = 4 (Sb3−La3 = 3.341 Å (2×), Sb3−La1 = 3.356 Å, Sb3−La1 = 3.360 Å; Sb5−La2 = 3.379 Å (2×), Sb5−La1 = 3.395 Å, Sb5−La3 = 3.404 Å); for the center Sb atoms (Sb4), CN = 4 (Sb4−La2 = 3.355 Å, Sb4−La1 = 3.384 Å (2×), Sb4−La3 = 3.386 Å). We can also estimate the bond length/bond strength of the Sb−Sb contacts in the stripes using Pauling's formula $d(n') = d_1 - 0.60$ Å $\log(n')$,[51] where n' is the bond order and $d_1 = 1.41$ Å for Sb. The sum of the calculated bond orders are therefore n(Sb2) = 1.30, n(Sb3) = 2.38, n(Sb4) = 2.28, n(Sb5) = 2.30, and n(Sb6) = 1.20. These values indicate that the outer Sb2 and Sb6 atoms are more negatively charged compared to the inner ones, and the corresponding empirical charges are Sb2: −1.70, Sb3: −0.62, Sb4: −0.72 Sb5: −0.70, and Sb6: −1.80.

Each Ln-capped Sb square net propagates infinitely in the [001] direction, but spans only two diagonal Sb squares perpendicular to the [001] direction (Figure 1). All Sb_4 square hollows are capped by Ln atoms alternately from above and below. These Sb atoms are therefore coordinated tetrahedrally to four Ln atoms. This structural feature is similar to that of many layered intermetallic compounds such as $BaAl_4$ and $ThCr_2Si_2$.[52,53]

Electronic Structure. Although it seems complex, the electronic structure of $Ln_9Sb_{16}X_3$ can be characterized by a five-center-six-electron interaction pattern similar to that in the intermetallic compounds $BaAl_4$ and $ThCr_2Si_2$[52,53] as revealed by our computational analysis for $La_9Sb_{16}Br_3$. The La−Sb slab in the crystal structure is formed from a Sb square lattice with La capped on the square hollows shown in Figure 1b. The electronic structure can be constructed in a way similar to that for $BaAl_4$. The interaction diagram for a $LaSb_4$ pyramid in the La−Sb stripe is shown in Figure 2. At a Sb_4 square hollow, each Sb atom contributes a sp^3 hybrid. The four sp^3 hybrids form four symmetry-adapted cyclobutadienoid molecular orbitals a_1, e, and b_2. They interact with the d orbitals of the capping La atoms. The symmetry-matched d orbitals are d_{z^2}, d_{xz}, d_{yz}, and d_{xy}. Because of the orbital directionality of d_{z^2}, d_{xz}, and d_{yz}, the interaction results in three stabilized orbitals of a_1 and e symmetry. The interaction between the b_2 orbital in the Sb_4 square and the La d_{xy} orbital is weak because the d_{xy} orbital does not point its lobes to the Sb_4 square. Thus, the resulting lower orbital is weakly bonding. This interaction pattern is nearly the same as that in the borane compound B_5H_9.[54] The most important feature of the interaction is that the three low-lying orbitals at each $LaSb_4$ pyramid can accommodate six electrons. Since each Sb atom in the pyramid contributes only one sp^3 hybrid, the six electrons actually count for a LaSb unit. For a subsequent electron-counting purpose, these six electrons can be assigned to the Sb atom as it is more electronegative than La.

(51) Pauling, L. *The Nature of the Chemical Bond*, Third Ed.; Cornell University Press: Ithaca, NY, 1967; p 246.

(52) Zheng, C.; Hoffmann, R. *Z. Naturforsch. B* **1986**, (41), 292.
(53) Zheng, C.; Hoffmann, R. *J. Am. Chem. Soc.* **1986**, *108*, 3078.
(54) Lipscomb, W. N. *Boron Hydrides*; Benjamin: New York, 1963.

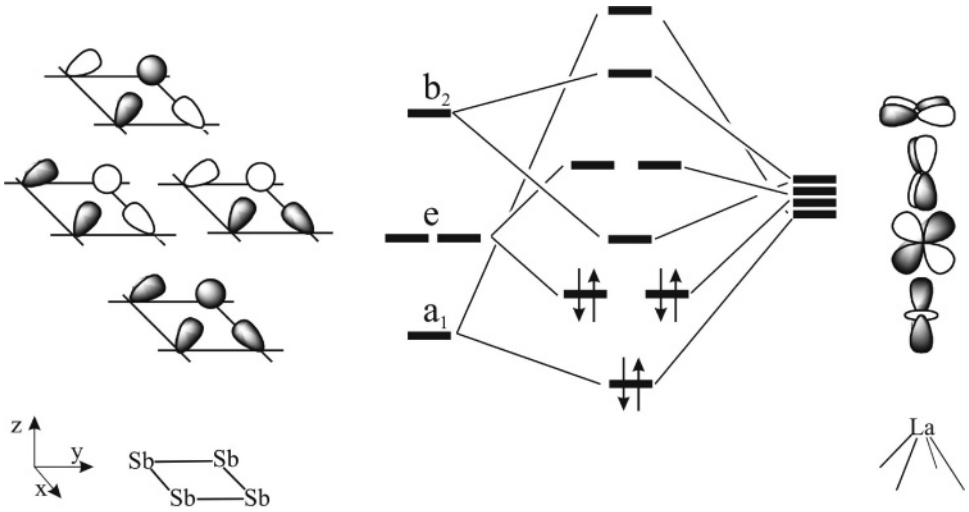

Figure 2. Interaction diagram for a $LaSb_4$ pyramid of the La-capped Sb square net. The Sb_4 base is at the left and the La apex at the right, resulting in three stabilized MO's in the middle accommodating six electrons.

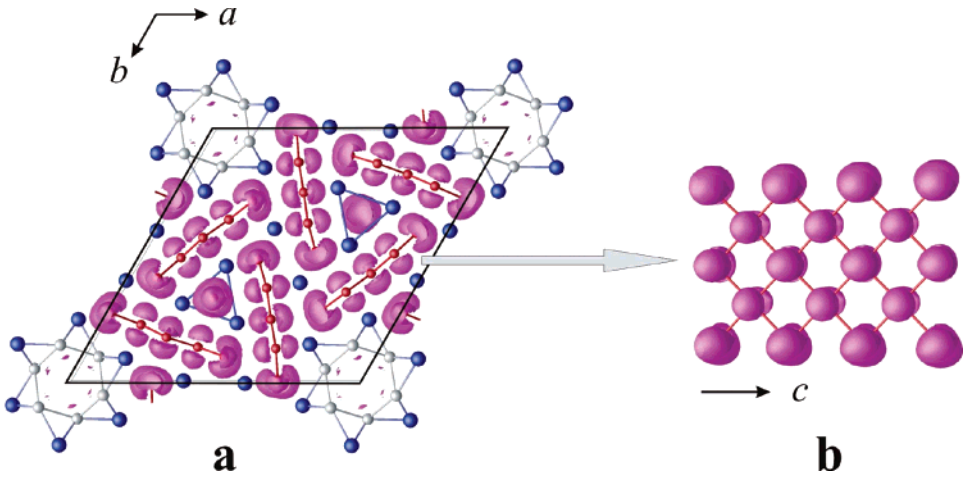

Figure 3. ELF surface at an isovalue of 0.75, computed by the LDA method for $Ln_9Sb_{16}Br_3$. (a) View down the *c*-axis. (b) View of a Sb stripe parallel to the *c*-axis.

Because of the electronegativity difference between Sb (2.05 in Pauling scale) and La (1.1), electrons are indeed localized at the Sb sites as confirmed by the ELF plot calculated by the LDA method in Figure 3. In this figure, the region of localized electrons is largest at the interstitial Sb (Sb_i) in the $[La_3Sb]_\infty$ trigonal prism; the next is at the edge Sb atoms of the La−Sb stripe. Therefore, when the missing Sb−Sb contacts along the edges of the La−Sb stripes are taken into account, the electron partitioning for $La_9Sb_{16}Br_3$ can be formulated as $(La^{3+})_9(Sb_e^{2-})_6(Sb_c^{-})_9(Sb_i^{3-})(Br^{-})_3$, where Sb_c^- has six valence electrons as prescribed above, Sb_e^{2-} on the La−Sb edges with missing bonds requires an extra electron, and Sb_i^{3-} in the $[La_3Sb]_\infty$ trigonal prism corresponds to a closed-shell electron configuration with no skeleton electrons in the La framework. The EH calculation supports such a scheme, as the edge Sb accumulate up to 0.6 more electron than the middle Sb atoms in the stripe. The electronic structure is again valence-precise in the $[La_6Br_6]_\infty$ hexagon star and the $[La_3Sb]_\infty$ trigonal prism, as in the Ln_3Ga_4Cl and $Ln_4M_5Br_2$ (Ln = La, Ce; M = Al, Ga) compounds synthesized by us previously.[55,56] As in those compounds, a reduced halide of this category can be valence-precise because the electron partition is only formal. For example, the assignment of Ga^{3-} for the three-connected Ga network in La_3Ga_4Cl will make this compound valence-precise. However, some of the electrons assigned to the rather electropositive, metallic Ga should reside in the La framework, resulting in a reduced La halide with metallic behavior. On the other side, the La−Sb stripe part is electron-deficient, possessing a five-center-six-electron bonding pattern. The example here illustrates that when the metal/metalloid-to-nonmetal ratio increases in the reduced rare earth halide system, a new type of compounds emerges. The hybrid material presented here has a reduced halide part that is valence-precise and an intermetallic component that is electron-deficient.

The computed DOS and COOP using the EH method are shown in Figures 4. In Figure 4a, the states immediately above −23 eV are mostly Br s orbitals followed by Sb s orbitals. Between −15 eV and −12 eV the states are a mixture of Br p and Sb p orbitals with minor participation

(55) Zheng, C.; Mattausch, Hj.; Simon, A. *Inorg. Chem.* **2003**, *42*, 3130.

(56) Zheng, C.; Mattausch, Hj.; Oeckler, O.; Nuss, J.; Simon, A. *Z. Anorg. Allg. Chem.* **2003**, *629*, 2229.

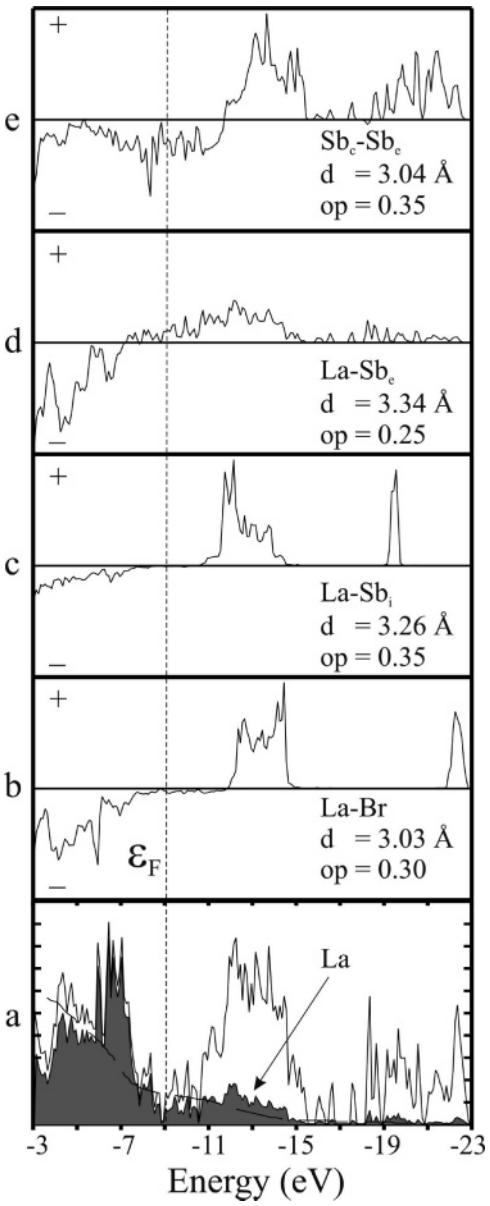

Figure 4. EH DOS and COOP plots for $La_9Sb_{16}Br_3$. (a) La DOS. The solid line is the total DOS, the dashed line the integrated La DOS, and the shaded area the contribution from La. The vertical dashed line indicates the Fermi level. (b−e) EH COOP curves for representative bonds in $La_9Sb_{16}Br_3$. The + region is bonding area and the − region antibonding area. The bond type, its distance (d), and integrated overlap population (op) to the Fermi level are indicated in the panel.

of La d orbitals. Because of the orbital interaction outlined in Figure 2, there is a pseudo gap near the Fermi level, leading to a metallic compound. The finite DOS in the pseudo gap is a result of extended interaction obscuring the division between the bonding and antibonding states. Above the Fermi level, the states are mostly La d orbitals. This indicates that La is mostly in a La^{3+} state for electron-counting purposes. Figure 4b shows that La−Br interaction is of bonding and localized character with distinctive Br s and p peaks. The same can be said of the La−Sb$_i$ interaction in the $[La_3Sb]_\infty$ trigonal prism (Figure 4c). The La−Sb$_e$, La−Sb$_c$ (the latter not shown but similar to Figure 4d), and Sb$_c$−Sb$_e$ interactions are much more delocalized as indicated by the spread in the COOP curves. They are mostly bonding except for the Sb$_c$−Sb$_e$ contact near the Fermi level due to the extended interaction in the La−Sb slab. These features are similar to those in the intermetallic compound $BaAl_4$. The La−La COOP curves demonstrate nonbonding interaction and are therefore not shown here. The DOS and COOP curves in this figure thus corroborate the interaction pattern presented in Figure 2.

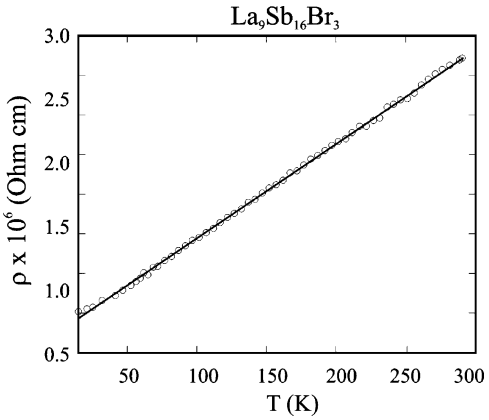

Figure 5. Resistivity of $La_9Sb_{16}Br_3$ measured in the temperature range 10−300 K (open circles) and its least-squares linear fit to 50 K (correlation coefficient = 0.9998).

Physical Properties. The resistivity of $La_9Sb_{16}Br_3$ measured in the temperature range 5−300 K shows a metallic behavior depicted in Figure 5. It exhibits a strictly linear temperature dependence down to 50 K. This corresponds to the DOS feature that there is strong La−Sb mixing and nonzero DOS at the Fermi level. Because of the extended interaction between unit cells and between the five-center-six-electron units in the La−Sb stripe, there is a strong mixing between the La d and the Sb p states. This mixing results in the metallic nature of the compound. Magnetic susceptibility measurement of $La_9Sb_{16}Br_3$ (not presented here) also shows a temperature-independent Pauli paramagnetism.

Acknowledgment. We thank R. Bailey for assisting the EDX measurements, E. Brücher for the magnetic susceptibility measurements, and G. Siegle for the conductivity measurements. C.Z. acknowledges the support by NSF through Grants DMR-9704048 and CHE-9974760, and by the Max-Planck-Gesellschaft which made his visit at MPI possible.

Supporting Information Available: Listing of X-ray crystallographic details in CIF format. This material is available free of charge via the Internet at http://pubs.acs.org.

IC049220U